applied sciences

MDPI

Article

Generation and Propagation of a Hermite-Gaussian Correlated Schell-Model LG_{0l} Beam

Xiaofeng Peng [1,†], Xingyuan Lu [1,†], Xianlong Liu [2], Chenliang Zhao [1], Rong Lin [2], Lin Liu [1,*] and Yangjian Cai [1,2,*]

1 School of Physical Science and Technology, Soochow University, Suzhou 215006, China; xfpeng888@163.com (X.P.); xylu_suda@163.com (X.L.); zhaochengliang@suda.edu.cn (C.Z.)
2 Shandong Provincial Engineering and Technical Center of Light Manipulations and Shandong Provincial Key Laboratory of Optics and Photonic Device, School of Physics and Electronics, Shandong Normal University, Jinan 250014, China; liuxianlong.ok@163.com (X.L.); hzxywlxlr@163.com (R.L.)
* Correspondence: liulin@suda.edu.cn (L.L.); yangjiancai@suda.edu.cn (Y.C.); Tel.: +86-139-1263-6612 (L.L.); +86-150-5015-7963 (Y.C.)
† These authors contributed equally to this work.

Received: 4 January 2019; Accepted: 8 February 2019; Published: 12 February 2019

Abstract: A partially coherent beam under the combined action of a Hermite-Gaussian correlated function and vortex phase, named the $HGCSMLG_{0l}$ beam has been explored both theoretically and experimentally. The statistical properties, such as the intensity and distribution of the degree of coherence (DOC) on propagation are analyzed in detail, based on the deduced equations. We find that the intensity is determined dominantly by the non-conventional correlated function when the coherence length is comparatively small and by vortex phase when the coherence length is large. The modulus of the DOC is not vulnerable to coherence width, rather, it is affected by both non-conventional correlated function and vortex phase. Our results are verified well by the experiment results.

Keywords: coherence and statistical optics; correlation function; topological charge; laser beam shaping

1. Introduction

The light beam with a spiral structure of the phase (i.e., vortex phase), named the vortex beam has continuously been under the spotlight in optical research area, due to its unique properties, e.g., orbital angular momentum (OAM), and phase singularity [1–3]. The OAM of a vortex beam can be used for particle trapping, detection of spinning object, free-space optical communications, and quantum information processing [4–7]. At the beginning, research attention was concentrated on the fully coherent vortex beams [8–11]. The quantitative measurement methods of the topological charge (TC) or the OAM state have been developed [12–17]. Until recently, a partially coherent (PC) beam, obtained by reducing the spatial coherence width, has demonstrated its superiority to a complete coherent counterpart in various applications [18–26]. In other words, controlling the spatial coherence width provides an effective way of manipulating beam properties. It is naturally to extend the coherent vortex beams to partially coherent vortex light (PCV). The PCV light, whose correlation function satisfies the Gaussian distribution, is a conventional PCV beam (e.g., Gaussian Schell-model (GSM) vortex light). Compared with PC light without vortex phase, and its complete coherent counterpart, the GSM vortex beam has advantages in many aspects. It can be shaped into prescribed beam profiles by modulating the coherence width of the incident beam to capture particles no matter which index of refraction is larger or smaller than that of the ambient [26,27]. PCV light has advantages of attenuating

the beam-width spreading, beam wander, and scintillation induced by atmospheric turbulence [28–30]. PCV light also displays self-reconstruction abilities in the distribution of the DOC on propagation, which can be used for information encryption and decryption [31].

Now, more and more attention has been paid to PC light with non-Gaussian distribution correlation function, which is named the special correlated (or nonconventional) PC light. A variety of these type of beams have been constructed and generated experimentally [20,32–39], ever since the conditions which guarantee the real existence of cross-spectral density function or matrix, were discussed in [40,41]. These non-Gaussian distribution correlation functions bring about the new changes and characteristics of the beam on propagation, which can be applied to reduce scintillation in turbulence and realize optical super resolution [42–44]. In this article, we will discuss the combined action of special correlation structure and the vortex phase on the beam's propagation properties, both theoretically and experimentally. An LG_{0l} beam with a Hermite-Gaussian correlated function named $HGCSMLG_{0l}$ beam is introduced and explored in detail. We find that the correlation function and TC together determine the focused spot and the DOC distribution on the propagation displays' rotating properties, which are induced by the vortex phase. By measuring the distribution of DOC, the handedness and the TC of the vortex phase can be obtained. The above theory results are verified well by the experiment results.

2. Propagation Equation of a $HGCSMLG_{0l}$ Beam

For a PC LG_{0l} beam, the cross-spectral density (CSD) function can be described as follows [45,46],

$$\boldsymbol{W}(\boldsymbol{r}_1, \boldsymbol{r}_2) = \left(\frac{2r_1 r_2}{4\sigma_0^2}\right)^{|l|} \exp\left(-\frac{\boldsymbol{r}_1^2 + \boldsymbol{r}_2^2}{4\sigma_0^2}\right) \gamma(\boldsymbol{r}_2 - \boldsymbol{r}_1) \exp[-il(\varphi_1 - \varphi_2)], \tag{1}$$

where $\boldsymbol{r}_1$, $\boldsymbol{r}_2$ are two arbitrary points in the source plane, σ_0, φ and l are the beam width, azimuth angle, and the topological charge, respectively, $\gamma(\boldsymbol{r}_2 - \boldsymbol{r}_1)$ denotes the correlation function. In order to explore the effects of a special correlation function on a PCV, the conventional Gaussian distribution function will be replaced by a Hermite-Gaussian distribution function, which can be expressed by:

$$\begin{aligned}\gamma(\boldsymbol{r}_2 - \boldsymbol{r}_1) = {} & \frac{H_{2m}\left[(x_2 - x_1)/\sqrt{2}\delta_0\right]}{H_{2m}[0]} \exp\left[-\frac{(x_2 - x_1)^2}{2\delta_0^2}\right] \\ & \times \frac{H_{2n}\left[(y_2 - y_1)/\sqrt{2}\delta_0\right]}{H_{2n}[0]} \exp\left[-\frac{(y_2 - y_1)^2}{2\delta_0^2}\right],\end{aligned} \tag{2}$$

where δ_0 is the spatial coherence width, H_{2m}, and H_{2n} are the Hermite polynomial with beam order $2m$, and $2n$, respectively. This new constructed beam is called the $HGCSMLG_{0l}$ beam.

According to the generalized Huygens-Fresnel principle [26,37], a $HGCSMLG_{0l}$ beam passing through an ABCD optical system can be dealt with the generalized Collins integral equation

$$\begin{aligned}\boldsymbol{W}(\boldsymbol{\rho}_1, \boldsymbol{\rho}_2; z) = {} & \frac{1}{(\lambda B)^2} \int_{-\infty}^{\infty} \int_{-\infty}^{\infty} W(r_1, r_2) \exp\Big\{-\frac{ik}{2B}\left[A\left(\boldsymbol{r}_1^2 - \boldsymbol{r}_2^2\right)\right. \\ & \left. - 2\boldsymbol{r}_1 \cdot \boldsymbol{\rho}_1 + 2\boldsymbol{r}_2 \cdot \boldsymbol{\rho}_2 + D\left(\rho_1^2 - \rho_2^2\right)\right]\Big\} d^2\boldsymbol{r}_1 d^2\boldsymbol{r}_2,\end{aligned} \tag{3}$$

where $\boldsymbol{\rho}_1$ and $\boldsymbol{\rho}_2$ are two arbitrary points in the output plane, k and A, B, D are the wave-number and the transfer matrix elements of an optical system.

By substituting Equations (1) and (2) into Equation (3) and the integrating them, the CSD of the outgoing $HGCSMLG_{0l}$ beam can be acquired with the intermediate steps listed in Appendix A.

$$W(\boldsymbol{\rho}_1,\boldsymbol{\rho}_2;z)=\Pi\sum_{c_1=0}^{|l|}\sum_{c_2=0}^{|l|}\sum_{k_1=0}^{m}\sum_{k_2=0}^{n}\sum_{p_1}^{2k_1}\sum_{p_2}^{2k_2}\sum_{d_1=0}^{b_4}\sum_{a_1=0}^{[d_1/2]}\sum_{d_2=0}^{b_2}\sum_{a_2=0}^{[d_2/2]}\left(\frac{1}{2\delta_0^2}\right)^{k_1+k_2}\left(\frac{i\sqrt{2}}{\sqrt{\alpha_1^*}\delta_0^2}\right)^{d_1+d_2-2a_1-2a_2}$$
$$\times\frac{(-1)^{b_6}(i)^{b_5}\pi^2 d_1!d_2!|l|!|l|!}{a_1!a_2!c_1!c_2!k_1!k_2!}\frac{2^{-3(b_2+b_4)/2-b_x-b_y}\left(\alpha_1^*\right)^{-(b_2+b_4+2)/2}\alpha_2{}^{-(b_x+by+2)/2}}{(d_1-2a_1)!(d_2-2a_2)!(|l|-c1)!(|l|-c2)!}$$
$$\times\binom{n-1/2}{n-k_2}\binom{m-1/2}{m-k_1}\binom{2k_2}{p_2}\binom{2k_1}{p_1}\binom{b_4}{d_1}\binom{b_2}{d_2}H\left(\rho_{x1},\rho_{x2},\rho_{y1},\rho_{y2}\right), \tag{4}$$

with

$$\Pi=\frac{1}{\left(2\sigma_0^2\right)^{|l|}\lambda^2B^2}\frac{m!\sqrt{\pi}}{\Gamma(m+1/2)}\frac{n!\sqrt{\pi}}{\Gamma(n+1/2)}\exp\left(-\frac{ikD}{2B}\left(\rho_1^2-\rho_2^2\right)\right), \tag{5}$$

$$H\left(\rho_{x1},\rho_{x2},\rho_{y1},\rho_{y2}\right)=H_{b_y}\left(i\frac{\beta_y}{2\sqrt{\alpha_2}}\right)H_{b_x}\left(\frac{i\beta_x}{2\sqrt{\alpha_2}}\right)H_{b_2-d_2}\left(\frac{k\rho_{x2}}{\sqrt{2\alpha_1^*B}}\right)$$
$$\times H_{b_4-d_1}\left(\frac{k\rho_{y2}}{\sqrt{2\alpha_1^*B}}\right)\exp\left(\frac{\beta_x^2+\beta_y^2}{4\alpha_2}\right)\exp\left(-\frac{k^2\left(\rho_{x2}^2+\rho_{y2}^2\right)}{4\alpha_1^*B^2}\right), \tag{6}$$

$$\begin{aligned}&b_1=|l|+p_1-c_1;\ b_2=|l|+2k_1-p_1-c_2,\ b_3=c_1+p_2;\\&b_4=c_2+2k_2-p_2;\ b_5=c_1+c_2-b_2-b_4-b_x-b_y;\\&b_6=a_1+a_2+k_1+k_2+p_1+p_2+c_\gamma,\ b_x=b_1+d_2-2a_2;\\&b_y=b_3+d_1-2a_1;\ c_\gamma=\begin{cases}c_1 & l\geq 0\\ c_2 & l<0\end{cases};\end{aligned} \tag{7}$$

$$\begin{aligned}&\alpha_1=\frac{1}{4\sigma_0^2}+\frac{1}{2\delta_0^2}+\frac{ikA}{2B};\ \alpha_2=\alpha_1-\frac{1}{4\alpha_1^*\delta_0^4};\ \beta_y=\frac{ik\rho_{y1}}{B}-\frac{ik\rho_{y2}}{2\alpha_1^*B\delta_0^2};\\&\beta_x=\frac{ik\rho_{x1}}{B}-\frac{ik\rho_{x2}}{2\alpha_1^*B\delta_0^2}.\end{aligned} \tag{8}$$

The intensity and the DOC of the HGCSMLG$_{0l}$ beam in the exiting plane are expressed as;

$$I(\boldsymbol{\rho},z)=W(\boldsymbol{\rho},\boldsymbol{\rho};z), \tag{9}$$

$$\mu(\boldsymbol{\rho}_1,\boldsymbol{\rho}_2;\mathrm{z})=\frac{W(\boldsymbol{\rho}_1,\boldsymbol{\rho}_2;z)}{\sqrt{W(\boldsymbol{\rho}_1,\boldsymbol{\rho}_1;z)W(\boldsymbol{\rho}_2,\boldsymbol{\rho}_2;z)}}. \tag{10}$$

Submitting Equations (4)–(8) into Equations (9)–(10), one can analyze the distributions of the intensity and the DOC of the propagating HGCSMLG$_{0l}$ beam conveniently.

3. Theoretical Analysis the Propagation of an HGCSMLG$_{0l}$ Beam

Applying the formulae obtained in the last section, the statistical properties of a propagating HGCSMLG$_{0l}$ beam will be analyzed. It is supposed that the beam propagates in free space after passing through a focal lens locating at $z=0$ with $f=400$ mm. The related parameters are defined as $\lambda=632.8$ nm,$\sigma_0=1$ mm, $\delta_0=1$ mm.

In Figures 1–3, we calculated the normalized intensity of a focused HGCSMLG$_{0l}$ beam at different distances with $m=0, n=1$ and the increasing values of the TC. One finds from the first row of Figures 1–3, that the HGCSMLG$_{0l}$ beam reduces to the HGCSM beam for $l=0$. As expected, a propagating HGCSM beam will split from the original one spot to four spots gradually [37]. From the second row and the third row of Figures 1–3, the HGCSMLG$_{0l}$ beam exhibits interesting variance of the beam profile under the combined action of unconventional correlation function and the vortex phase. As the second row of Figures 1–3 shows, the intensity distribution of the HGCSMLG0l beam evolves increasingly from a donut shape into a two-beamlets array distribution (see Figures 1d2 and 2d2) or four-beamlets array distribution (see Figure 3d2) in the focal plane, while a PC LG$_{0l}$ beam remains in a circular symmetry while propagating in free space [45,46]. It is clear that the new special correlation function plays a dominant role in the transmission rule of the beam. As the third row of Figures 1–3 shows, the light spot of the focal plane does not separate into two (or four) beamlets with the increasing TC. It can be explained that the vortex phase plays an anti-splitting role.

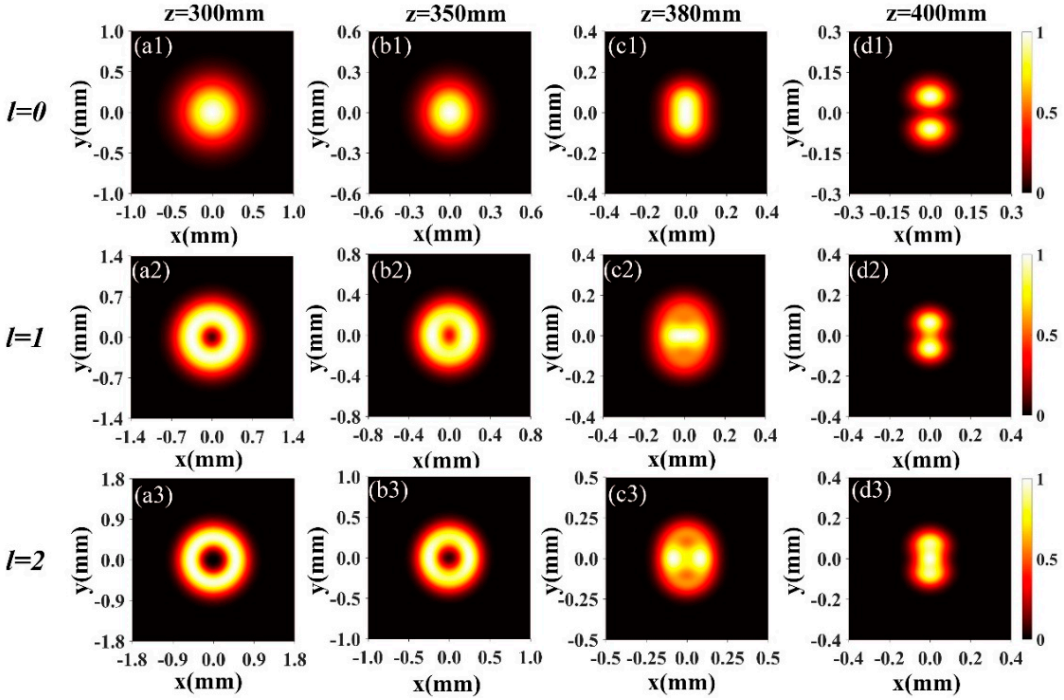

Figure 1. Normalized intensity of a focused HGCSMLG$_{0l}$ beam at different distances with $m = 0$, $n = 1$ and increasing values of the TC.

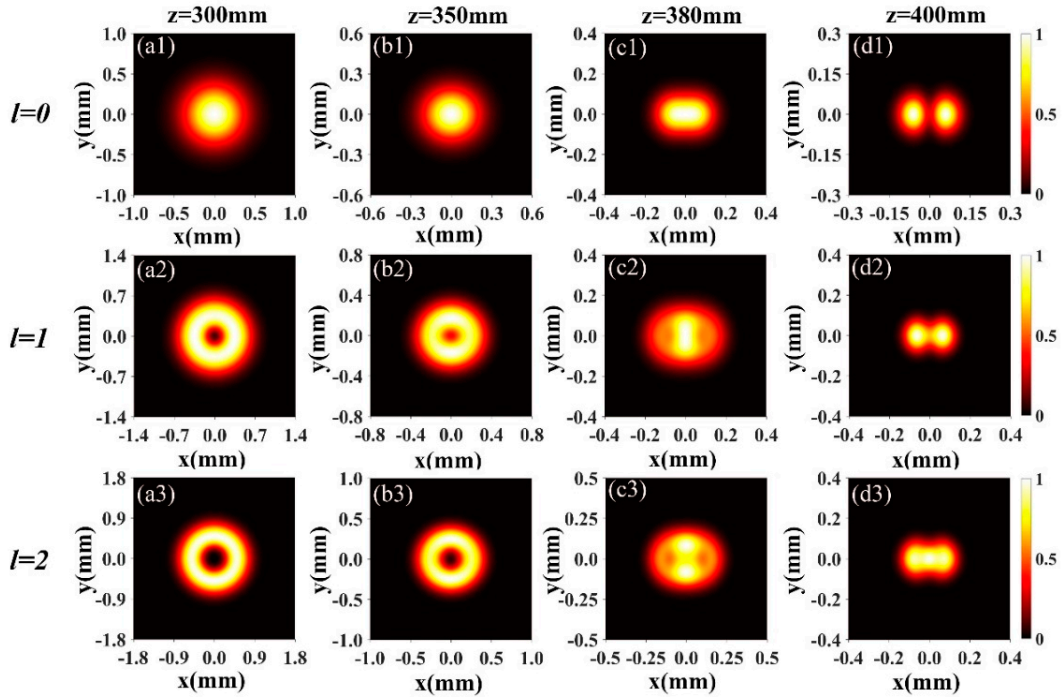

Figure 2. Normalized intensity of a focused HGCSMLG$_{0l}$ beam at different distances with $m = 0$, $n = 1$ and increasing values of the topological charge (TC).

Figure 4 shows the normalized focal plane intensity of an HGCSMLG$_{0l}$ beam, with $l = 2$ for different beam orders m, n and the spatial coherence width δ_0. One can see that the beam orders m, n and the spatial coherence width δ_0 determine the splitting array form of focal plane. Once the spatial coherence width δ_0 increases to a certain value, the far-field beamlets array distribution would disappear and degenerate into a semi-dark hollow beam profile. We can draw a conclusion that the

beam shape in the focal plane depends on the correlation function, as the initial coherence width is not large, and as the initial coherence width becomes large the focused beam profile is mainly determined by the vortex phase. As a result, coherence width should be suitably chosen to obtain the splitting array form of beam profile on propagation.

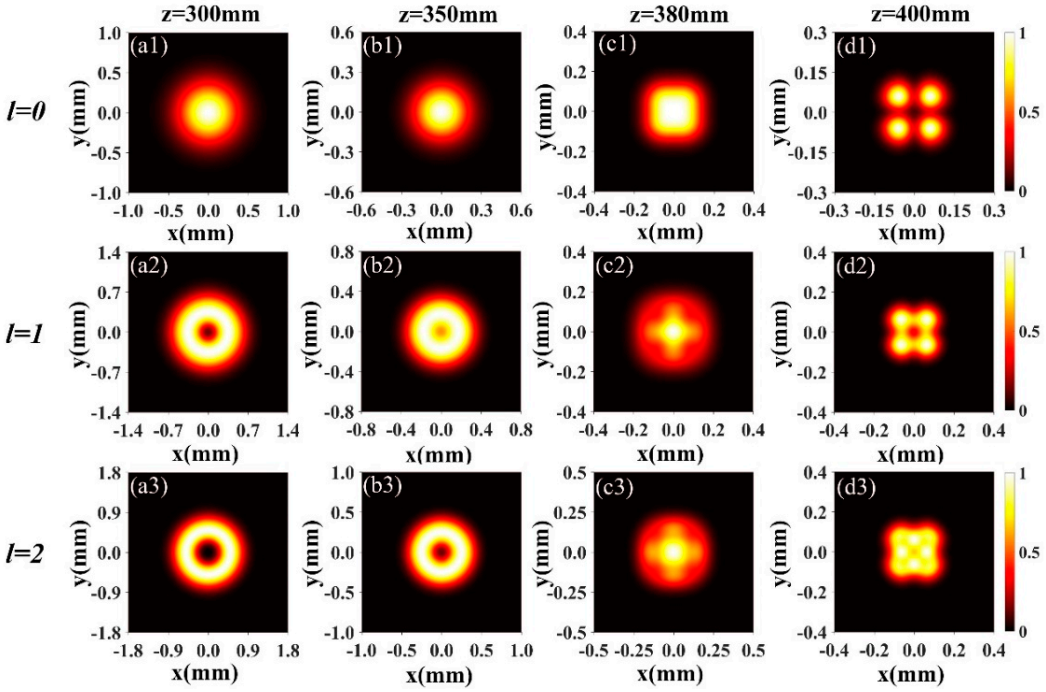

Figure 3. Normalized intensity of a focused HGCSMLG$_{0l}$ beam at different distances with $m = 1$, $n = 1$ and increasing values of the TC.

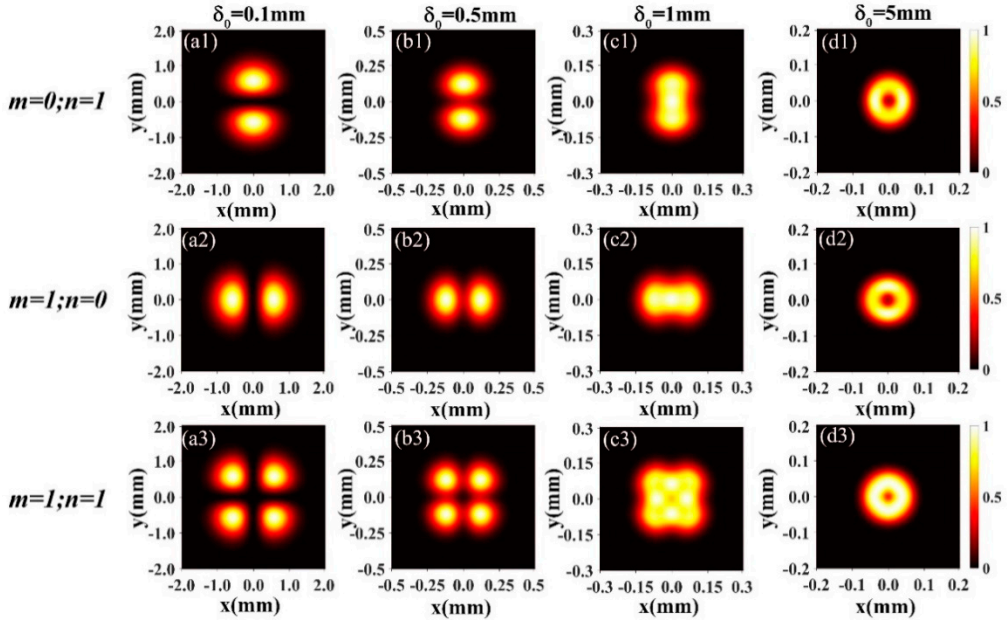

Figure 4. Normalized focal plane intensity of an HGCSMLG$_{0l}$ beam with $l = 2$ for different beam orders m, n and the spatial coherence width δ_0.

Figures 5–7 displays the modulus of the DOC ($|\mu(\boldsymbol{\rho}, 0; z)|$) of a focused HGCSMLG$_{0l}$ beam at different distances with different m, n and the increasing values of the TC. The first rows of Figures 5–7 show that the variation of the modulus of the DOC of a focused HGCSM beam, for different beam

order, with increasing distance z. The distribution of the DOC of the HGCSM beam displays an array distribution near the source plane ($z = 1$ mm) which is the same as the source plane [19] and remains array distribution as the beam propagates. It is not until it reaches the focal plane that the DOC distribution evolves into one beam spot. The second and the third rows of Figures 5–7 show the propagation properties of the DOC of a focused HGCSMLG$_{0l}$ beam at different distances for different beam order m, n and increasing values of the TC. One can find the vortex phase brings about obvious changes of the DOC distribution even in the plane ($z = 1$ mm) near the source plane. The DOC distribution exhibits a "rotating effect" as the beam propagates along the z axis. We can decide the handedness of the TC by the rotation direction of the distribution of the DOC. As the rotation direction of windmills (see Figure 7b2–c2) is anti-clockwise, the value of TC is positive ($l > 0$). While on the contrary, the value of TC is negative ($l < 0$) (see Figure 7b3–c3).

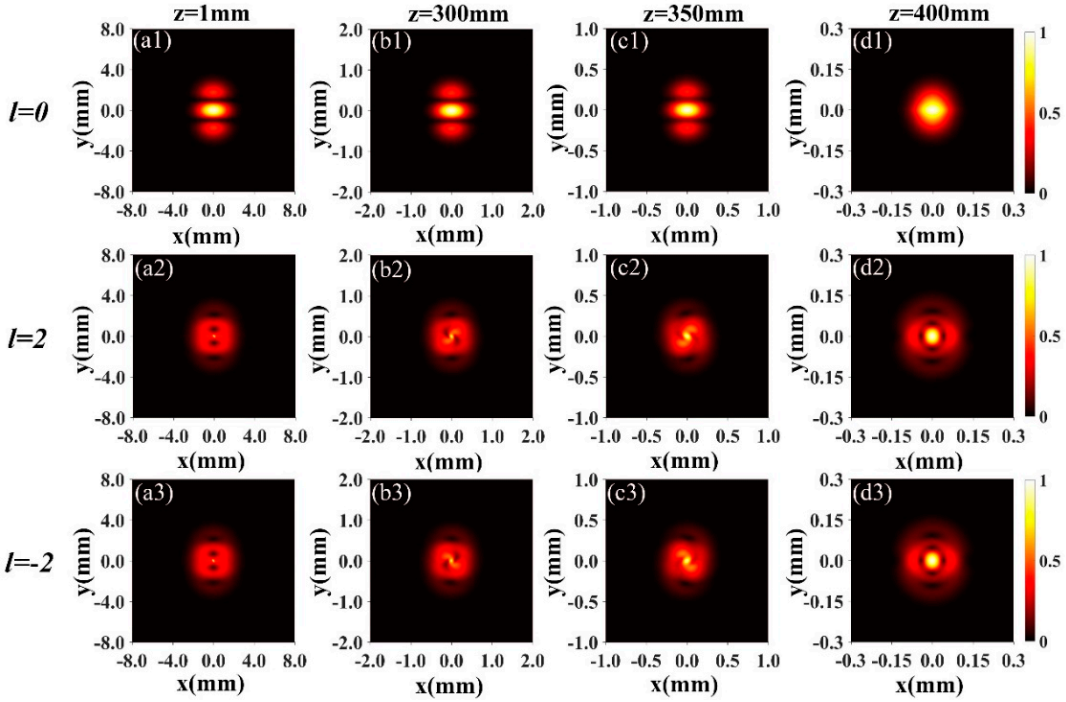

Figure 5. The modulus of the DOC ($|\mu(\boldsymbol{\rho}, 0; z)|$) of a focused HGCSMLG$_{0l}$ beam at different distances with $m = 0$, $n = 1$ and increasing values of the TC.

Figure 8 shows the modulus of the focal plane DOC of an HGCSMLG$_{0l}$ beam for different m, n and the TC. The dark rings' number of the focal plane DOC increases as the value of TC increases. For $m = 0$, $n = 1$ (see Figure 8a1–d1) and $m = 1$, $n = 0$ the dark rings' number along the y direction and the x direction equals to the TC number l separately. For $m = 1$, $n = 1$ (see Figure 8a3–d3), the dark rings' number along the x or y direction is one less than the TC number l if $l > 2$. Thus, the TC number can be determined by the number of the dark rings. It can be concluded that we can distinguish the handedness and value of the TC from the DOC distribution, in spite of form changes of the DOC distribution, caused by the new correlation function.

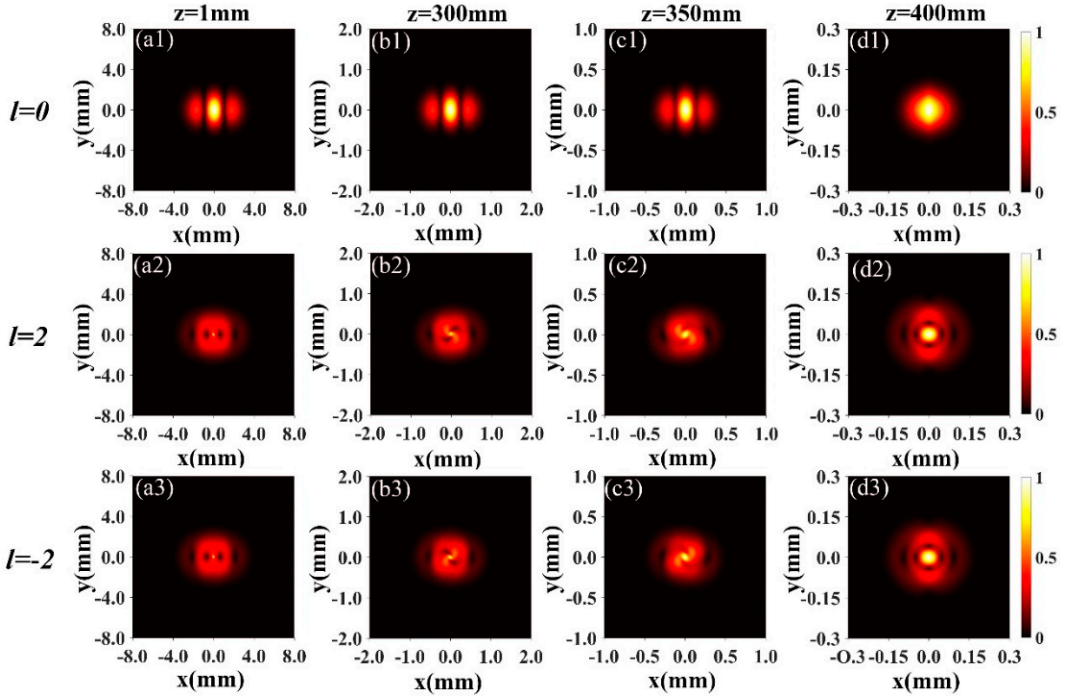

Figure 6. The modulus of the DOC ($|\mu(\boldsymbol{\rho}, 0; z)|$) of a focused HGCSMLG$_{0l}$ beam at different distances with $m = 1$, $n = 0$ and increasing values of the TC.

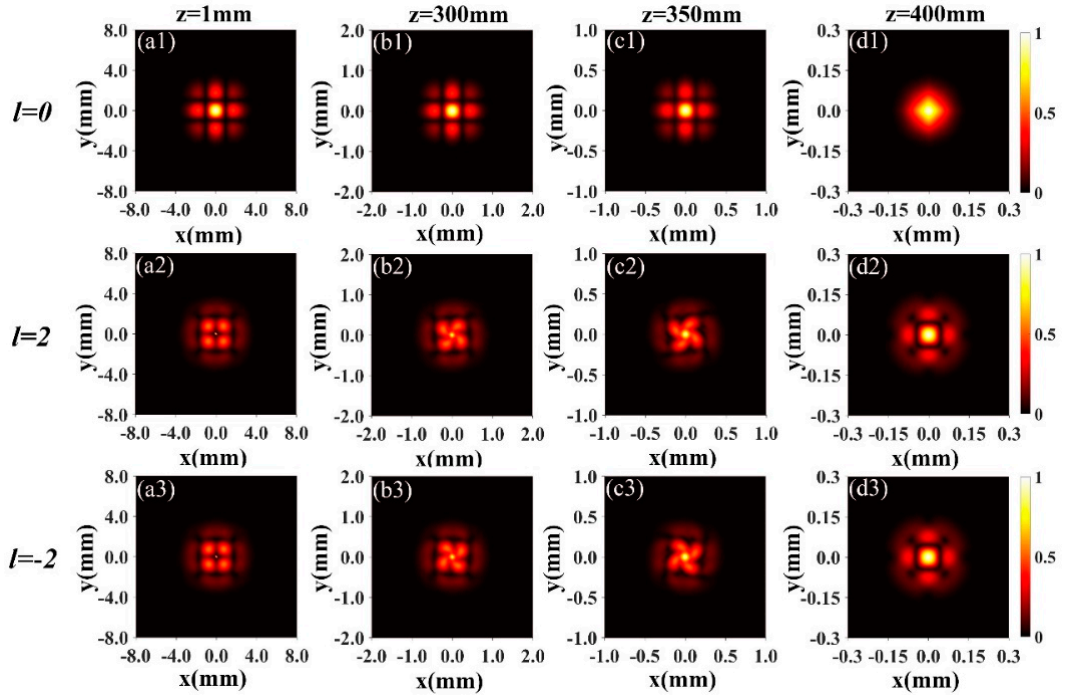

Figure 7. The modulus of the DOC ($|\mu(\boldsymbol{\rho}, 0; z)|$) of a focused HGCSMLG$_{0l}$ beam at different distances with $m = 1$, $n = 1$ and increasing values of the TC.

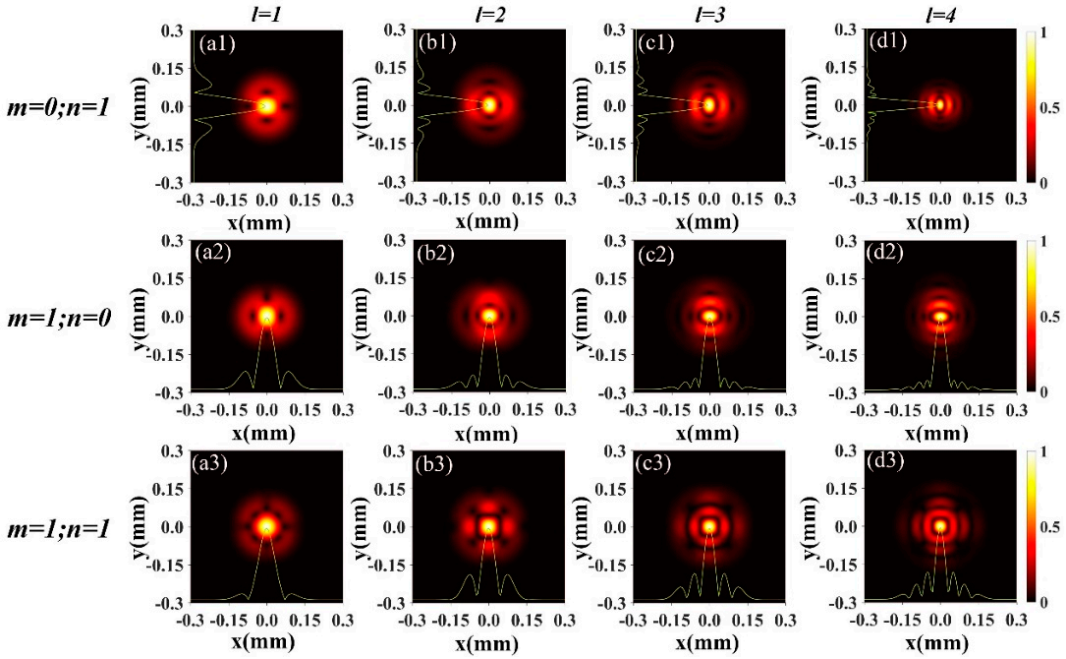

Figure 8. The modulus of the focal plane DOC ($|\mu(\boldsymbol{\rho}, 0; z)|$) of an HGCSMLG$_{0l}$ beam for different m, n and the TC. For the first row the solid curve is the cross line $x = 0$. For the second and third row the solid curve is the cross line $y = 0$.

4. Experimental Verification

In this part, the generation of an HGCSMLG$_{0l}$ beam is introduced and our theoretical predictions will be validated.

Figure 9 shows the optical layout for generating and measuring HGCSMLG$_{0l}$. For generating a HGCSMLG$_{0l}$ beam, the coherent laser beam, with λ = 532 nm comes into beam expander (BE) and the emitted light is modulated by spatial light modulator (SLM1). A designed computer-generated hologram, for producing the unconventional correlation function, is loaded on SLM1 [37]. The diffracted light of first-order is focused onto a rotating ground glass disk with lens (L1, f = 150 mm). The scattered light is collected by a lens (L2, f = 200 mm) and is then filtered by a Gaussian amplitude plate. SLM2 is a phase spatial light modulator which is used to loading the designed computer-generated holograms for generating the vortex phase. After SLM2, we can obtain the HGCSMLG$_{0l}$ beam. The TC and the beam orders m, n can be controlled by SLM2 and SLM1 separately. L3 is used to focus the generated HGCSMLG$_{0l}$ beam. The beam profile analyzer is used to record the intensity information of the measured plane. The corresponding correlation function can be measured with the help of self-referencing holography, as mentioned in Ref. [47], in which the correlation function of the illumination source can be retrieved.

Figure 10 shows our experimental results in relation to the intensity of a focused HGCSMLG$_{0l}$ beam at different distances for different beam orders m, n with $l = 2$. As can be seen, the new unconventional correlation function has a decisive role in the intensity evolution properties of the HGCSMLG0l beam.

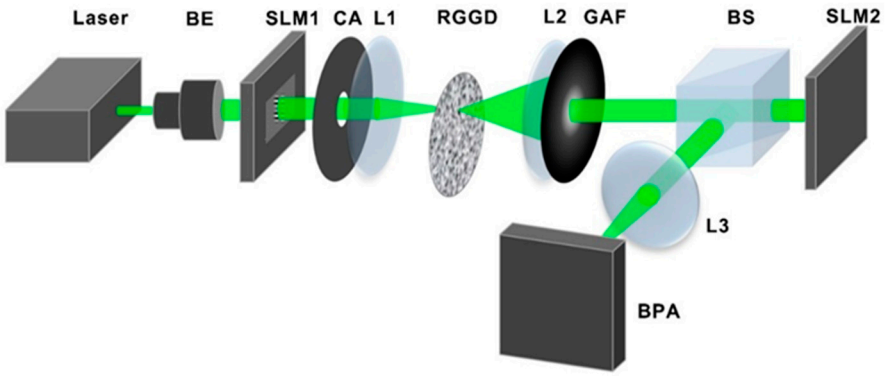

Figure 9. A scheme of optical layout for generating and measuring HGCSMLG$_{0l}$. Laser, 532 nm; BE, beam expander; SLM1, SLM2, spatial light modulator; CA, circular aperture; L1, L2, L3, lenses; RGGD, rotating ground glass disk; GAF, Gaussian amplitude filter; BS, beam splitter; BPA, beam profile analyzer.

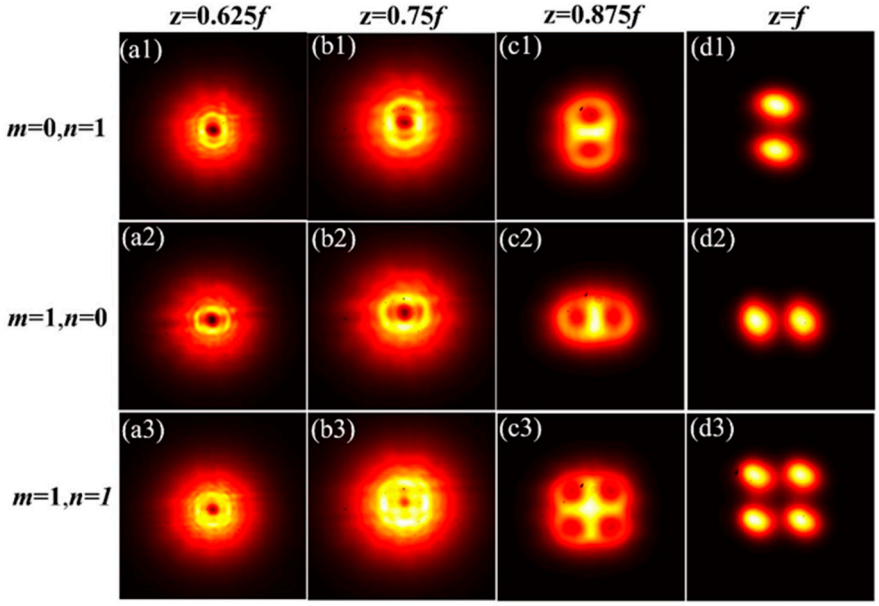

Figure 10. Experimental result of the intensity of a focused HGCSMLG$_{0l}$ beam at different distances for different beam orders m, n with $l = 2$.

The intensity distribution morphs from a donut shape into an array form on propagation, which agrees well with Figure 3. Figure 11 shows the measured modulus of the DOC ($|\mu(\boldsymbol{\rho}, 0; z)|$) of a focused HGCSMLG0l beam at $z = 0.68f$, with $m = 1, n = 1$ compared with the theoretical results. We find that the distribution of the DOC displays a "rotating effect". For $l > 0$ and $l < 0$, the direction of rotation is anti-clockwise and clockwise severally. So, the handedness of the vortex phase can be judged by measuring its DOC on propagation. Compared with the theoretical results, Figure 12 shows the measured modulus of the focal plane DOC of an HGCSMLG$_{0l}$ beam with $l = 2$ for different beam orders m, n. It can be found that the distribution of the DOC is dependent on the Hermite polynomial beam orders. For $m = 0$ and $n = 0$, the modulus of the DOC exhibits an elliptical distribution with the major axis along the y direction, and along x direction, respectively. For $m = 1, n = 1$, the distribution of the DOC has a rectangular distribution. Figure 13 shows the experimental modulus of the focal plane DOC of an HGCSMLG0l beam with $m = 1, n = 1$ and increasing values of TC. With the TC increasing, the dark rings' number of the modulus of the focal plane DOC also increases as shown in Figure 8. Thus, we can determine the magnitude of the TC by measuring its DOC in the focal plane. In general, our experimental results agree well with the theoretical results.

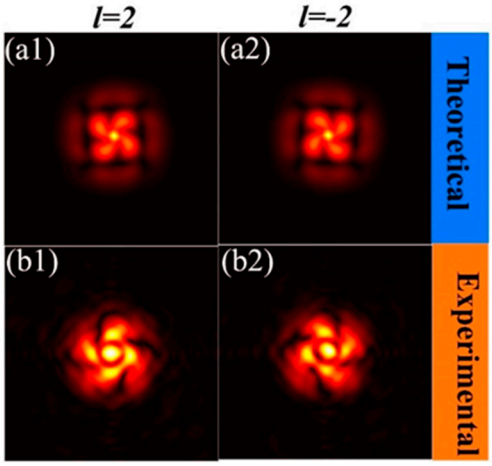

Figure 11. The modulus of the DOC ($|\mu(\boldsymbol{\rho}, 0; z)|$) of a focused HGCSMLG$_{0l}$ beam at $z = 0.68f$ with $m = 1, n = 1$.

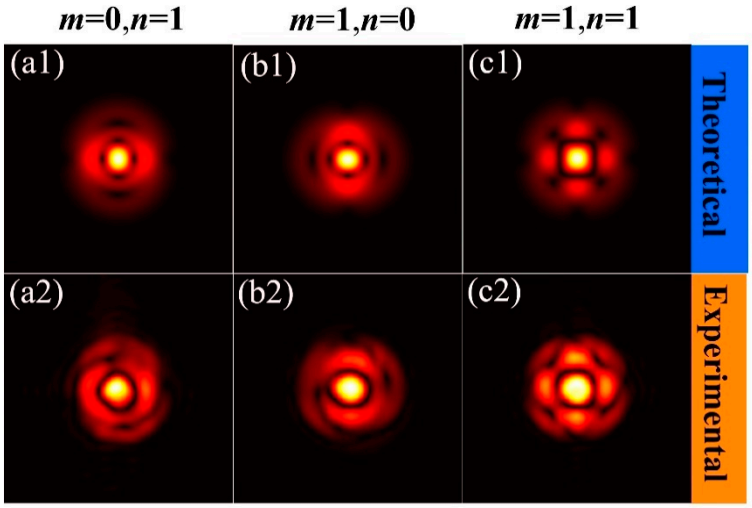

Figure 12. The modulus of the focal plane DOC ($|\mu(\boldsymbol{\rho}, 0)|$) of an HGCSMLG$_{0l}$ beam with $l = 2$ for different beam orders m, n.

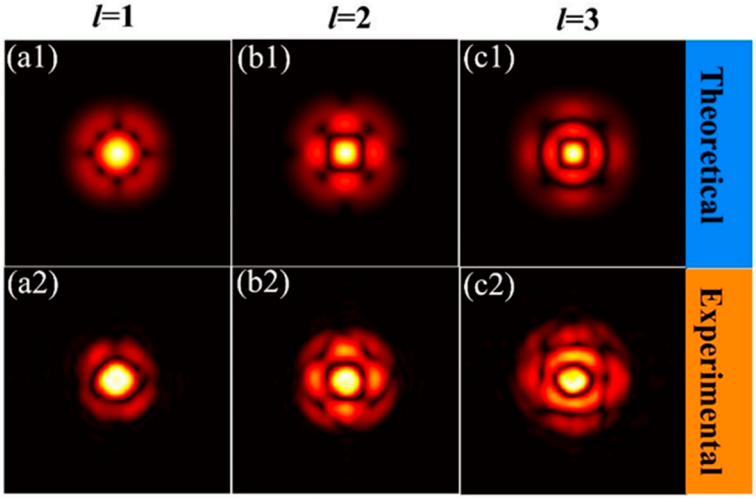

Figure 13. The modulus of the focal plane DOC ($|\mu(\boldsymbol{\rho}, 0)|$) of an HGCSMLG$_{0l}$ beam with $m = 1, n = 1$ and increasing values of TC.

5. Conclusions

Under interaction of nonconventional correlated function and vortex phase, the propagation rules of a partially coherent beam named HGCSMLG$_{0l}$ beam are investigated theoretically and experimentally. Our results show that the behavior of the intensity of the beam on propagation is determined by the vortex phase, spatial coherence width and correlation function of the initial beam together. When the spatial coherence width of the initial beam is large, the vortex phase plays a dominant role, and the beam spot in the focal plane still displays a dark hollow beam profile, which can be used for trapping a particle with refractive index smaller than that of the ambient. When the spatial coherence width of the initial beam is small, the correlation function plays a dominant role. The beam spot in the focal plane displays two or four solid beam spots, which can be used for trapping multiple particles simultaneous with refractive indices larger than that of the ambient. For the effect of the coherence width on the modulus of the DOC is not as obvious as the intensity distribution, the modulus of the DOC is affected by both non-conventional correlated function and vortex phase. In spite of the form change of the modulus of the DOC caused by the non-conventional correlated function, the handedness and TC of vortex phase can be distinguished from the modulus of the DOC. The robust of the handedness, and TC of vortex phase, which is not vulnerable to coherence length and correlation function, may be useful in information transfer and recovery.

Author Contributions: Data curation, X.P., X.L. (Xingyuan Lu); writing (original draft), X.P., X.L. (Xingyuan Lu); writing, X.L. (Xianlong Liu), R.L, L.L., and Y.C.; supervision, C.Z., L.L., and Y.C.; project administration, Y.C. All authors read and approved the final manuscript.

Funding: This work was supported by the National Natural Science Foundation of China (91750201, 11525418, 11774251, 11774250, 11804198); the Project of the Priority Academic Program Development (PAPD) of Jiangsu Higher Education Institutions.

Conflicts of Interest: The authors declare no conflict of interest.

Appendix A

The cross-spectral density (CSD) of the HGCSMLG$_{0l}$ beam in the source plane is defined as

$$\begin{aligned} \boldsymbol{W}(\boldsymbol{r}_1,\boldsymbol{r}_2) = \left(\frac{2r_1r_2}{4\sigma_0^2}\right)^{|l|} \exp\left(-\frac{r_1^2+r_2^2}{4\sigma_0^2}\right) \exp[-il(\varphi_1-\varphi_2)] \frac{H_{2m}\left[(x_2-x_1)/\sqrt{2}\delta_0\right]}{H_{2m}(0)} \\ \times \frac{H_{2n}\left[(y_2-y_1)/\sqrt{2}\delta_0\right]}{H_{2n}(0)} \exp\left[-\frac{(x_2-x_1)^2}{2\delta_0^2}\right] \exp\left[-\frac{(y_2-y_1)^2}{2\delta_0^2}\right], \end{aligned} \tag{A1}$$

Using the following expansion

$$H_{2n}(x) = (-1)^n 2^{2n} n! L_n^{-1/2}\left(x^2\right) \tag{A2}$$

$$L_n^{\alpha}(x) = \sum_{m=0}^{n} (-1)^m \begin{pmatrix} n+\alpha \\ n-m \end{pmatrix} \frac{x^m}{m!}; L_n^{\alpha}(0) = \frac{\Gamma(n+\alpha+1)}{n!\Gamma(\alpha+1)} \tag{A3}$$

$$(x \pm iy)^{|l|} = \sum_{c1=0}^{|l|} \frac{|l|!(\pm i)^{c1}}{c1!(|l|-c1)!} x^{|l|-c1} y^{c1} \tag{A4}$$

After some operation, Equation (A1) can be expressed in the following alternative form:

$$\begin{aligned} W(\boldsymbol{r}_1,\boldsymbol{r}_2) = \left(\frac{1}{2\sigma_0^2}\right)^{|l|} \frac{\mathrm{m}!\sqrt{\pi}}{\Gamma(m+1/2)} \frac{n!\sqrt{\pi}}{\Gamma(n+1/2)} \sum_{c1=0}^{|l|} \sum_{c2=0}^{|l|} (-1)^{c_i} \frac{|l|!(i)^{c1}}{c1!(|l|-c1)!} \frac{|l|!i^{c2}}{c2!(|l|-c2)!} \\ \times x_1^{|l|-c1} x_2^{|l|-c2} {y_1}^{c1} {y_2}^{c2} \exp\left[-\frac{r_1^2+r_2^2}{4\sigma_0^2}\right] L_m^{-1/2}\left(\frac{(x_2-x_1)^2}{2\delta_0^2}\right) L_n^{-1/2}\left(\frac{(y_2-y_1)^2}{2\delta_0^2}\right) \\ \times \exp\left[-\frac{(x_2-x_1)^2}{2\delta_0^2}\right] \exp\left[-\frac{(y_2-y_1)^2}{2\delta_0^2}\right], (l \geq 0, c_i = c_1; l < 0, c_i = c_2) \end{aligned} \tag{A5}$$

With the help of the generalized Huygens-Fresnel integral, the propagation of a HGCSMLG$_{0l}$ beam through an ABCD optical system can be treated by the following generalized Collins integral formula:

$$\begin{aligned}\boldsymbol{W}(\boldsymbol{\rho}_1,\boldsymbol{\rho}_2;z) = \tfrac{1}{(\lambda B)^2}\int_{-\infty}^{\infty}\int_{-\infty}^{\infty} W(r_1,r_2)\exp\Big\{-\tfrac{ik}{2B}\big[A\big(\boldsymbol{r}_1^2-\boldsymbol{r}_2^2\big)\\ -2\boldsymbol{r}_1\cdot\boldsymbol{\rho}_1+2\boldsymbol{r}_2\cdot\boldsymbol{\rho}_2+D\big(\rho_1^2-\rho_2^2\big)\big]\Big\}d^2\boldsymbol{r}_1 d^2\boldsymbol{r}_2,\end{aligned} \tag{A6}$$

Substituting Equation (A5) with Equation (A6), after some tedious integration and operation, we obtained the analytical formula for the CSD of a HGCSMLG$_{0l}$ beam in the output plane as:

$$\begin{aligned}\boldsymbol{W}(\boldsymbol{\rho}_1,\boldsymbol{\rho}_2;z) = \Pi\sum_{c_1=0}^{|l|}\sum_{c_2=0}^{|l|}\sum_{k_1=0}^{m}\sum_{k_2=0}^{n}\sum_{p_1}^{2k_1}\sum_{p_2}^{2k_2}\sum_{d_1=0}^{b_4}\sum_{a_1=0}^{[d_1/2]}\sum_{d_2=0}^{b_2}\sum_{a_2=0}^{[d_2/2]}\left(\tfrac{1}{2\delta_0^2}\right)^{k_1+k_2}\left(\tfrac{i\sqrt{2}}{\sqrt{\alpha_1^*}\delta_0^2}\right)^{d_1+d_2-2a_1-2a_2}\\ \times\tfrac{(-1)^{b_6}(i)^{b_5}\pi^2 d_1!d_2!|l|!|l|!}{a_1!a_2!c_1!c_2!k_1!k_2!}\tfrac{2^{-3(b_2+b_4)/2-b_x-b_y}\left(\alpha_1^*\right)^{-(b_2+b_4+2)/2}\alpha_2^{-(b_x+by+2)/2}}{(d_1-2a_1)!(d_2-2a_2)!(|l|-c1)!(|l|-c2)!}\\ \times\binom{n-1/2}{n-k_2}\binom{m-1/2}{m-k_1}\binom{2k_2}{p_2}\binom{2k_1}{p_1}\binom{b_4}{d_1}\binom{b_2}{d_2}H\big(\rho_{x1},\rho_{x2},\rho_{y1},\rho_{y2}\big),\end{aligned} \tag{A7}$$

With

$$\Pi = \frac{1}{\left(2\sigma_0^2\right)^{|l|}\lambda^2B^2}\frac{m!\sqrt{\pi}}{\Gamma(m+1/2)}\frac{n!\sqrt{\pi}}{\Gamma(n+1/2)}\exp\left(-\frac{ikD}{2B}\left(\rho_1^2-\rho_2^2\right)\right), \tag{A8}$$

$$\begin{aligned}H\big(\rho_{x1},\rho_{x2},\rho_{y1},\rho_{y2}\big) = H_{b_y}\left(i\tfrac{\beta_y}{2\sqrt{\alpha_2}}\right)H_{b_x}\left(\tfrac{i\beta_x}{2\sqrt{\alpha_2}}\right)H_{b_2-d_2}\left(\tfrac{k\rho_{x2}}{\sqrt{2\alpha_1^*B}}\right)\\ \times H_{b_4-d_1}\left(\tfrac{k\rho_{y2}}{\sqrt{2\alpha_1^*B}}\right)\exp\left(\tfrac{\beta_x^2+\beta_y^2}{4\alpha_2}\right)\exp\left(-\tfrac{k^2\left(\rho_{x2}^2+\rho_{y2}^2\right)}{4\alpha_1^*B^2}\right),\end{aligned} \tag{A9}$$

$$\begin{aligned}&b_1 = |l|+p_1-c_1;\ b_2 = |l|+2k_1-p_1-c_2,\ b_3 = c_1+p_2;\\ &b_4 = c_2+2k_2-p_2;\ b_5 = c_1+c_2-b_2-b_4-b_x-b_y;\\ &b_6 = a_1+a_2+k_1+k_2+p_1+p_2+c_\gamma,\ b_x = b_1+d_2-2a_2;\\ &b_y = b_3+d_1-2a_1;\ c_\gamma = \begin{cases} c_1 & l\geq 0\\ c_2 & l<0\end{cases};\end{aligned} \tag{A10}$$

$$\begin{aligned}\alpha_1 = \tfrac{1}{4\sigma_0^2}+\tfrac{1}{2\delta_0^2}+\tfrac{ikA}{2B};\ \alpha_2 = \alpha_1-\tfrac{1}{4\alpha_1^*\delta_0^4};\\ \beta_y = \tfrac{ik\rho_{y1}}{B}-\tfrac{ik\rho_{y2}}{2\alpha_1^*B\delta_0^2};\beta_x = \tfrac{ik\rho_{x1}}{B}-\tfrac{ik\rho_{x2}}{2\alpha_1^*B\delta_0^2}.\end{aligned} \tag{A11}$$

In above derivations, we have used the following expansion and integral formulae:

$$\int_{-\infty}^{\infty}x^\alpha\exp\left[-(x-\beta)^2\right]dx = (2i)^{-\alpha}\sqrt{\pi}H_\alpha(i\beta) \tag{A12}$$

$$H_\alpha(x+\beta) = \frac{1}{2^{\alpha/2}}\sum_{p=0}^{\alpha}\binom{\alpha}{p}H_p\left(\sqrt{2}x\right)H_{\alpha-p}\left(\sqrt{2}\beta\right) \tag{A13}$$

$$H_n(x_1) = \sum_{m=0}^{[n/2]}(-1)^m\frac{n!}{m!(n-2m)!}(2x_1)^{n-2m} \tag{A14}$$

References

1. Soskin, M.S.; Vasnetsov, M.V. Singular optics. In *Progress in Optics*; Wolf, E., Ed.; Elsevier: Amsterdam, The Netherlands, 2001; Volume 42, pp. 219–276, ISBN 978-0-444-50908-6.
2. Born, M.; Wolf, E. *Principles of Optics*; Cambridge University Press: Cambridge, UK, 1999; ISBN 978-0-521-64222-4.
3. Nye, J.F.; Berry, M.V. Dislocations in wave trains. *Proc. R. Soc. Lond. A* **1974**, *336*, 1605. [CrossRef]
4. Gahagan, K.T.; Swartzlander, G.A. Optical vortex trapping of particles. *Opt. Lett.* **1996**, *21*, 827–829. [CrossRef] [PubMed]

5. Gibson, G.; Courtial, J.; Padgett, M.; Vasnetsov, M.; Pas'ko, V.; Barnett, S.; Franke-Arnold, S. Free-space information transfer using light beams carrying orbital angular momentum. *Opt. Express* **2004**, *12*, 5448–5456. [CrossRef] [PubMed]
6. Lavery, M.P.J.; Speirits, F.C.; Barnett, S.M.; Padgett, M.J. Detection of a spinning object using light's orbital angular momentum. *Science* **2013**, *341*, 537–540. [CrossRef] [PubMed]
7. Vaziri, A.; Pan, J.W.; Jennewein, T.; Weihs, G.; Zeilinger, A. Concentration of higher dimensional entanglement: Qutrits of photon orbital angular momentum. *Phys. Rev. Lett.* **2003**, *91*, 227902. [CrossRef] [PubMed]
8. Flossmann, F.; Schwarz, U.T.; Maier, M. Propagation dynamics of optical vortices in Laguerre–Gaussian beams. *Opt. Commun.* **2005**, *250*, 218–230. [CrossRef]
9. Orlov, S.; Regelskis, K.; Smilgevičius, V.; Stabinis, A. Propagation of Bessel beams carrying optical vortices. *Opt. Commun.* **2002**, *209*, 155–165. [CrossRef]
10. Yang, Y.; Dong, Y.; Zhao, C.; Cai, Y. Generation and propagation of an anomalous vortex beam. *Opt. Lett.* **2013**, *38*, 5418–5421. [CrossRef] [PubMed]
11. Vaity, P.; Rusch, L. Perfect vortex beam: Fourier transformation of a Bessel beam. *Opt. Lett.* **2015**, *40*, 597–600. [CrossRef]
12. Berkhout, G.C.G.; Beijersbergen, M.W. Method for probing the orbital angular momentum of optical vortices in electromagnetic waves from astronomical objects. *Phys. Rev. Lett.* **2008**, *101*, 100801. [CrossRef] [PubMed]
13. Sztul, H.I.; Alfano, R.R. Double-slit interference with Laguerre-Gaussian beams. *Opt. Lett.* **2006**, *31*, 999–1001. [CrossRef] [PubMed]
14. de Araujo, L.E.E.; Anderson, M.E. Measuring vortex charge with a triangular aperture. *Opt. Lett.* **2011**, *36*, 787–789. [CrossRef] [PubMed]
15. Vinu, R.V.; Singh, R.K. Determining helicity and topological structure of coherent vortex beam from laser speckle. *Appl. Phys. Lett.* **2016**, *109*, 111108. [CrossRef]
16. Prabhakar, S.; Kumar, A.; Banerji, J.; Singh, R.P. Revealing the order of a vortex through its intensity record. *Opt. Lett.* **2011**, *36*, 4398–4400. [CrossRef] [PubMed]
17. Zhao, P.; Li, S.; Feng, X.; Cui, K.; Liu, F.; Zhang, W.; Huang, Y. Measuring the complex orbital angular momentum spectrum of light with a mode-matching method. *Opt. Lett.* **2017**, *42*, 1080–1083. [CrossRef] [PubMed]
18. Cai, Y.; Chen, Y.; Yu, J.; Liu, X.; Liu, L. Generation of Partially Coherent Beams. *Prog. Opt.* **2017**, *62*, 157–223. [CrossRef]
19. Wang, F.; Liu, X.; Yuan, Y.; Cai, Y. Experimental generation of partially coherent beams with different complex degrees of coherence. *Opt. Lett.* **2013**, *38*, 1814–1816. [CrossRef] [PubMed]
20. Cai, Y.; Chen, Y.; Wang, F. Generation and propagation of partially coherent beams with nonconventional correlation functions: A review [Invited]. *J. Opt. Soc. Am. A* **2014**, *31*, 2083–2096. [CrossRef] [PubMed]
21. Kato, Y.; Mima, K.; Miyanaga, N.; Arinaga, S.; Kitagawa, Y.; Nakatsuka, M.; Yamanaka, C. Random phasing of high-power lasers for uniform target acceleration and plasma-instability suppression. *Phys. Rev. Lett.* **1984**, *53*, 1057–1060. [CrossRef]
22. Ricklin, J.C.; Davidson, F.M. Atmospheric turbulence effects on a partially coherent Gaussian beam: Implications for free-space laser communication. *J. Opt. Soc. Am. A* **2002**, *19*, 1794–1802. [CrossRef]
23. Wang, F.; Liu, X.; Cai, Y. Propagation of partially coherent beam in turbulent atmosphere: A review (Invited review). *Prog. Electromagn. Res.* **2015**, *150*, 123–143. [CrossRef]
24. Cai, Y.; Zhu, S.Y. Ghost imaging with incoherent and partially coherent light radiation. *Phys. Rev. E* **2005**, *71*, 056607. [CrossRef] [PubMed]
25. Liu, X.; Wang, F.; Zhang, M.; Cai, Y. Effects of atmospheric turbulence on lensless ghost imaging with partially coherent light. *Appl. Sci.* **2018**, *8*, 1479. [CrossRef]
26. Zhao, C.; Cai, Y. Trapping two types of particles using a focused partially coherent elegant Laguerre-Gaussian beam. *Opt. Lett.* **2011**, *36*, 2251–2253. [CrossRef] [PubMed]
27. Wang, F.; Zhu, S.; Cai, Y. Experimental study of the focusing properties of a Gaussian Schell-model vortex beam. *Opt. Lett.* **2011**, *36*, 3281–3283. [CrossRef] [PubMed]
28. Liu, X.; Shen, Y.; Liu, L.; Wang, F.; Cai, Y. Experimental demonstration of vortex phase-induced reduction in scintillation of a partially coherent beam. *Opt. Lett.* **2013**, *38*, 5323–5326. [CrossRef]

29. Wu, G.; Dai, W.; Tang, H.; Guo, H. Beam wander of random electromagnetic Gaussian-shell model vortex beams propagating through a Kolmogorov turbulence. *Opt. Commun.* **2015**, *336*, 55–58. [CrossRef]
30. Li, J.; Lü, B. Propagation of Gaussian Schell-model vortex beams through atmospheric turbulence and evolution of coherent vortices. *J. Opt. A* **2009**, *11*, 045710. [CrossRef]
31. Liu, X.; Peng, X.; Liu, L.; Wu, G.; Zhao, C.; Wang, F.; Cai, Y. Self-reconstruction of the degree of coherence of a partially coherent vortex beam obstructed by an opaque obstacle. *Appl. Phys. Lett.* **2017**, *110*, 181104. [CrossRef]
32. Liang, C.; Wang, F.; Liu, X.; Cai, Y.; Korotkova, O. Experimental generation of cosine Gaussian correlated Schell-model beams with rectangular symmetry. *Opt. Lett.* **2014**, *39*, 769–772. [CrossRef]
33. Chen, Y.; Cai, Y. Generation of a controllable optical cage by focusing a Laguerre–Gaussian correlated Schell-model beam. *Opt. Lett.* **2014**, *39*, 2549–2552. [CrossRef] [PubMed]
34. Lajunen, H.; Saastamoinen, T. Propagation characteristics of partially coherent beams with spatially varying correlations. *Opt. Lett.* **2011**, *36*, 4104–4106. [CrossRef] [PubMed]
35. Yu, J.; Cai, Y.; Gbur, G. Rectangular Hermite non-uniformly correlated beams and its propagation properties. *Opt. Express* **2018**, *26*, 27894–27906. [CrossRef] [PubMed]
36. Liang, C.; Zhu, X.; Mi, C.; Peng, X.; Wang, F.; Cai, Y.; Ponomarenko, S.A. High-quality partially coherent Bessel beam array generation. *Opt. Lett.* **2018**, *43*, 3188–3191. [CrossRef] [PubMed]
37. Chen, Y.; Gu, J.; Wang, F.; Cai, Y. Self-splitting properties of a Hermite-Gaussian correlated Schell-model beam. *Phys. Rev. A* **2015**, *91*, 013823. [CrossRef]
38. Ma, L.; Ponomarenko, S.A. Free-space propagation of optical coherence lattices and periodicity reciprocity. *Opt. Express* **2015**, *23*, 1848–1856. [CrossRef]
39. Liu, X.; Liu, L.; Wang, F.; Cai, Y. Generation of a flexible far-field anomalous hollow beam spot through superposition of two partially coherent sources with different degrees of coherence. *Opt. Commun.* **2018**, *428*, 69–76. [CrossRef]
40. Gori, F.; Santarsiero, M. Devising genuine spatial correlation functions. *Opt. Lett.* **2007**, *32*, 3531–3533. [CrossRef]
41. Gori, F.; Sanchez, V.R.; Santarsiero, M.; Shirai, T. On genuine cross-spectral density matrices. *J. Opt. A Pure Appl. Opt.* **2009**, *11*, 085706. [CrossRef]
42. Yuan, Y.; Liu, X.; Wang, F.; Chen, Y.; Cai, Y.; Qu, J.; Eyyuboglu, H.T. Scintillation index of a multi-Gaussian Schell-model beam in turbulent atmosphere. *Opt. Commun.* **2013**, *305*, 57–65. [CrossRef]
43. Gu, Y.; Gbur, G. Scintillation of nonuniformly correlated beams in atmospheric turbulence. *Opt. Lett.* **2013**, *38*, 1395–1397. [CrossRef] [PubMed]
44. Liang, C.; Wu, G.; Wang, F.; Li, W.; Cai, Y.; Ponomarenko, S.A. Overcoming the classical Rayleigh diffraction limit by controlling two-point correlations of partially coherent light sources. *Opt. Express* **2017**, *25*, 28352–28362. [CrossRef]
45. Wang, F.; Cai, Y.; Korotkova, O. Partially coherent standard and elegant Laguerre-Gaussian beams of all orders. *Opt. Express* **2009**, *17*, 22366–22379. [CrossRef] [PubMed]
46. Zhao, C.; Wang, F.; Dong, Y.; Han, Y.; Cai, Y. Effect of spatial coherence on determining the topological charge of a vortex beam. *Appl. Phys. Lett.* **2012**, *101*, 261104. [CrossRef]
47. Shao, Y.; Lu, X.; Konijnenberg, S.; Zhao, C.; Cai, Y.; Urbach, H.P. Spatial coherence measurement and partially coherent diffractive imaging using self-referencing holography. *Opt. Express* **2018**, *26*, 4479–4490. [CrossRef] [PubMed]